Supplementary material

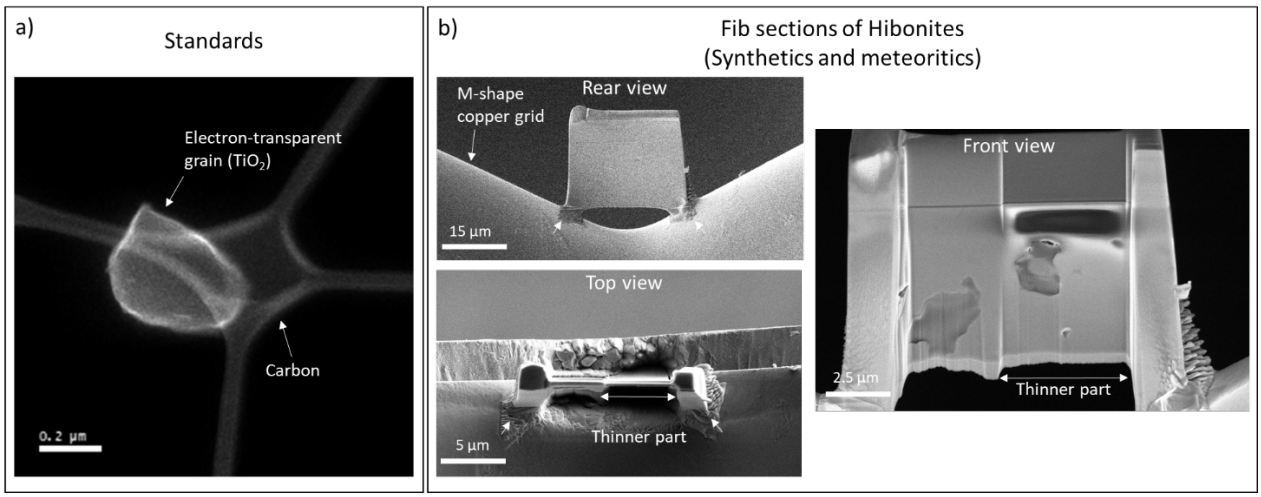

Figure S1: a) HAADF STEM image of the crushed powder (here TiO_2) deposited on Cu TEM grid supporting a lacey carbon film. All the standards are prepared through the same protocol. Only electron-transparent grains (carbon membrane visible below the grain) were selected. B) FIB images (BSE and SE) showing how the section is mounted on the M-shaped post to limit bending during thinning. We ion milled a small part of the sample to minimize the bending.

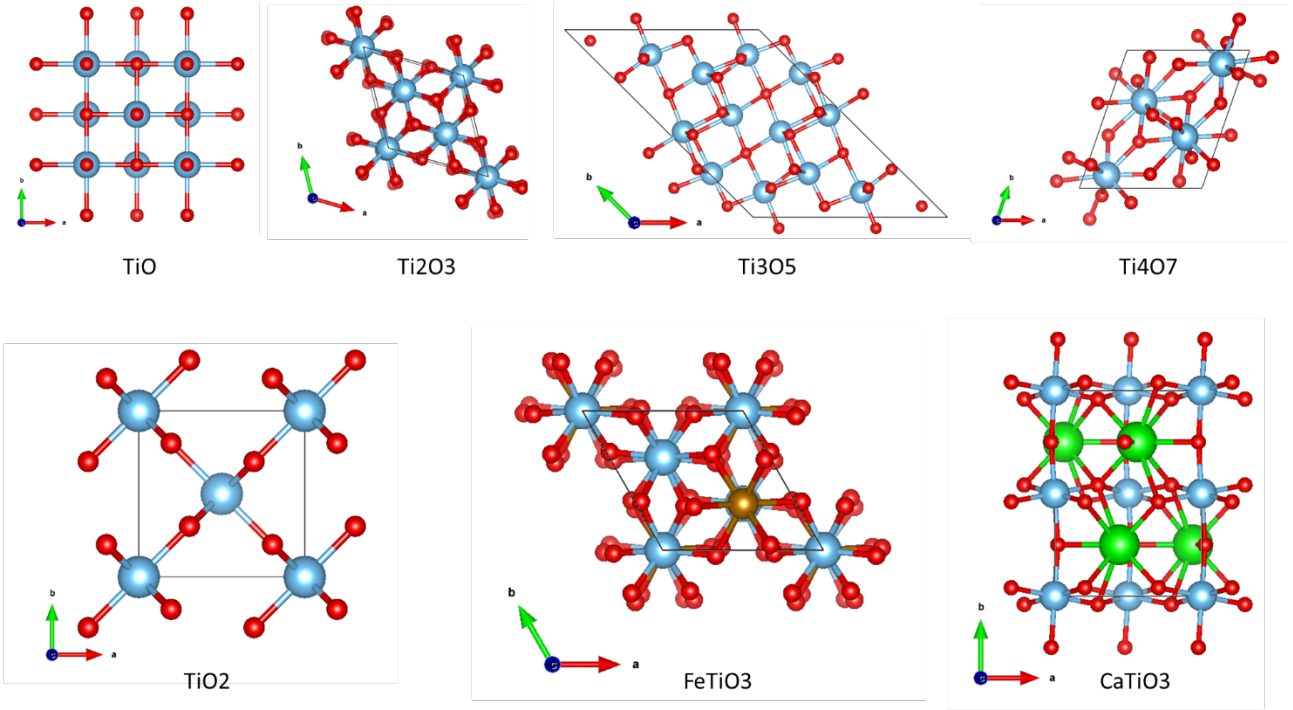

Figure S2: Ball-and-stick atomic-structure models of the standards measured in this work as shown in c-axis projections. Atoms are; red: oxygen, blue: aluminum, green: titanium and orange:Fe.

			TiO	TiO_2
Peak	Transition		Number of e^- in the final state	Number of e^- in the final state
a	$2p_{3/2} \rightarrow 2t_{2g}$	L_3	2 → Weaker	0
b	$2p_{3/2} \rightarrow 3e_g$	L_3	0	0
c	$2p_{1/2} \rightarrow 2t_{2g}$	L_2	2 → Weaker	0
d	$2p_{1/2} \rightarrow 3e_g$	L_2	0	0

Table S1: Possible electronic transitions between inner core electronic states to empty states above E_f. The higher occupancy of the $2t_{2g}$ level is at the origin of the lower intensity of the peak a and c in TiO.

	$TiL_{2,3}$ edge peak positions (eV) - This work						TiL_3 edge peak positions (eV) - Stoyanov et al., 2007			
Oxides	a	b'	b	c	d'	d	a	a'	b	b'
$CaTiO_3$	458.18	-	460.50	463.63	-	465.90	-	-	-	-
$FeTiO_3$	458.35	-	460.70	463.79	-	466.27	-	-	-	-
TiO_2 (Rutile)	458.18	459.96	461.09	463.79	465.58	466.17	458.30	-	460.00	460.80
Ti_4O_7	458.03	-	459.86	463.58	-	465.47	456.60	-	459.50	-
Ti_3O_5	456.40	458.29	459.32	461.96	463.90	464.76	456.40	-	459.00	-
Ti_2O_3	456.57	458.88	459.54	462.18	464.12	464.71	456.30	458.10	458.90	-
TiO	455.65	-	458.03	461.53	-	463.25	-	-	457.40	-

Table S2: Experimentally determined energy positions of the peaks a, b, b', c, d, and d' within $L_{2,3}$ edges of Ti-oxides. Comparison with previous peak positions within L_3 edges from (Stoyanov et al., 2007)

	TiL2,3 edge peak positions (eV)					
Oxides	a	b'	b	c	c'	d
ALL 2-6	457.88	459.70	460.46	463.31	463.90	465.78
All 2-57	458.29	459.95	460.81	463.69	464.31	465.99
ALL 2-55	458.09	459.89	460.46	463.23	463.66	465.87
NWA 5028	457.94	459.55	460.38	463.31	463.80	465.78

Table S3: Experimentally determined energy positions of the peaks a, b, b', c, c', and d' within $L_{2,3}$ edges of synthetic and natural hibonites.

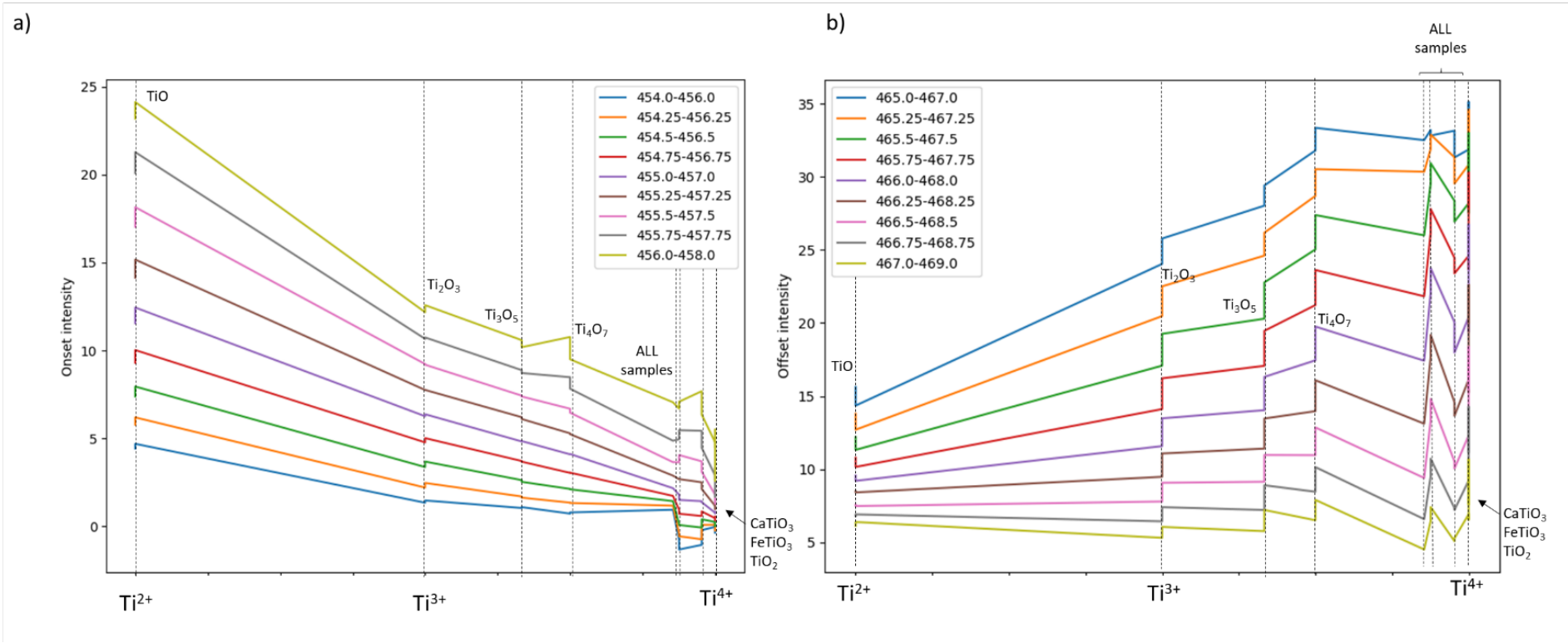

Figure S3: 2 eV edge onset and offset window position and resulting fit. a) Determination of the best onset-window position. The best linear fit (lower point dispersion) is obtained for 455-457 eV. b) The same procedure is applied to the offset window position. However, a significant dispersion is observed for any position and this precludes its use for establishing a relationship between the Ti oxidation state and the IL_2/IL_3 ratio.

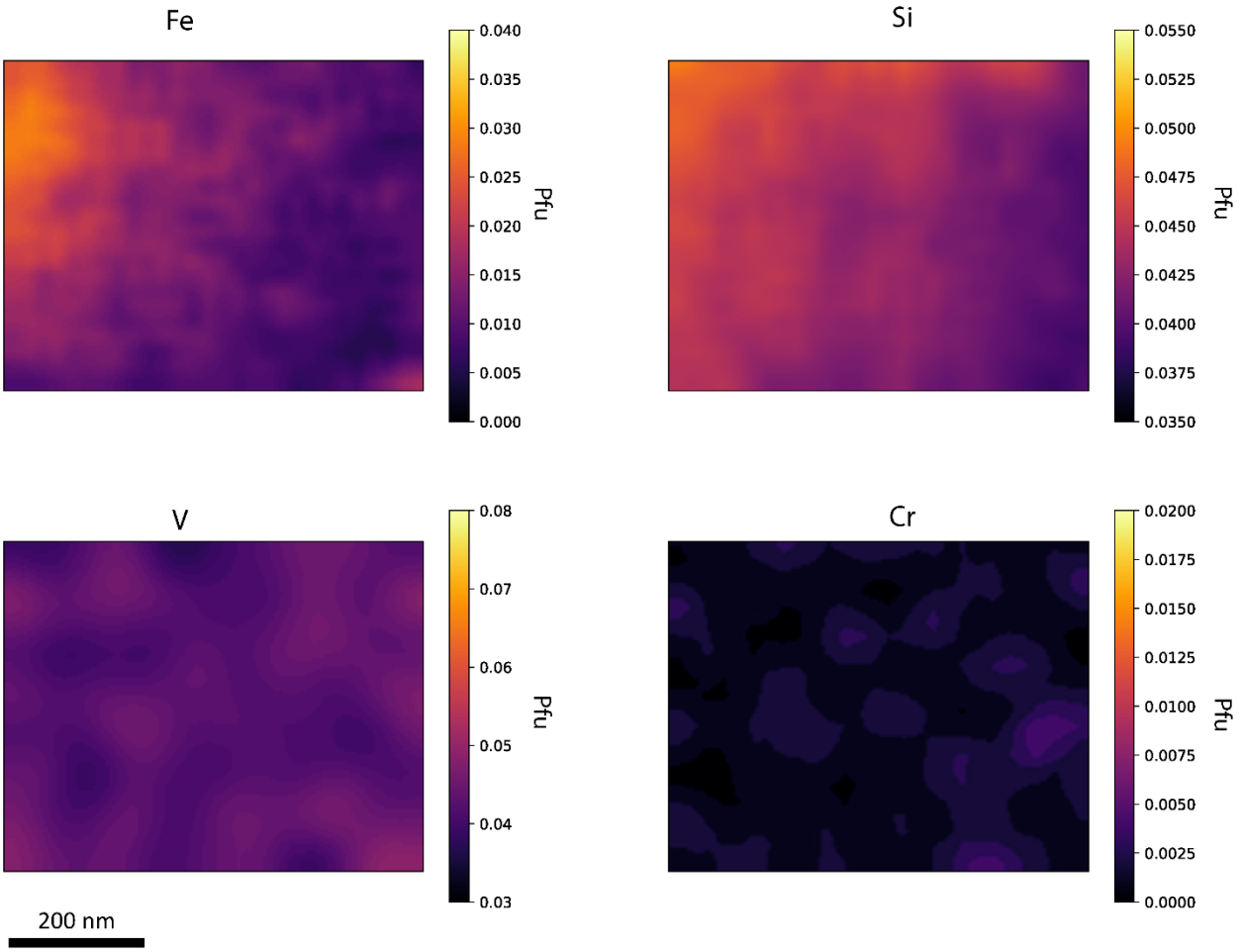

Figure S4: Quantified EDS maps of the minor elements in the hibonite grain.

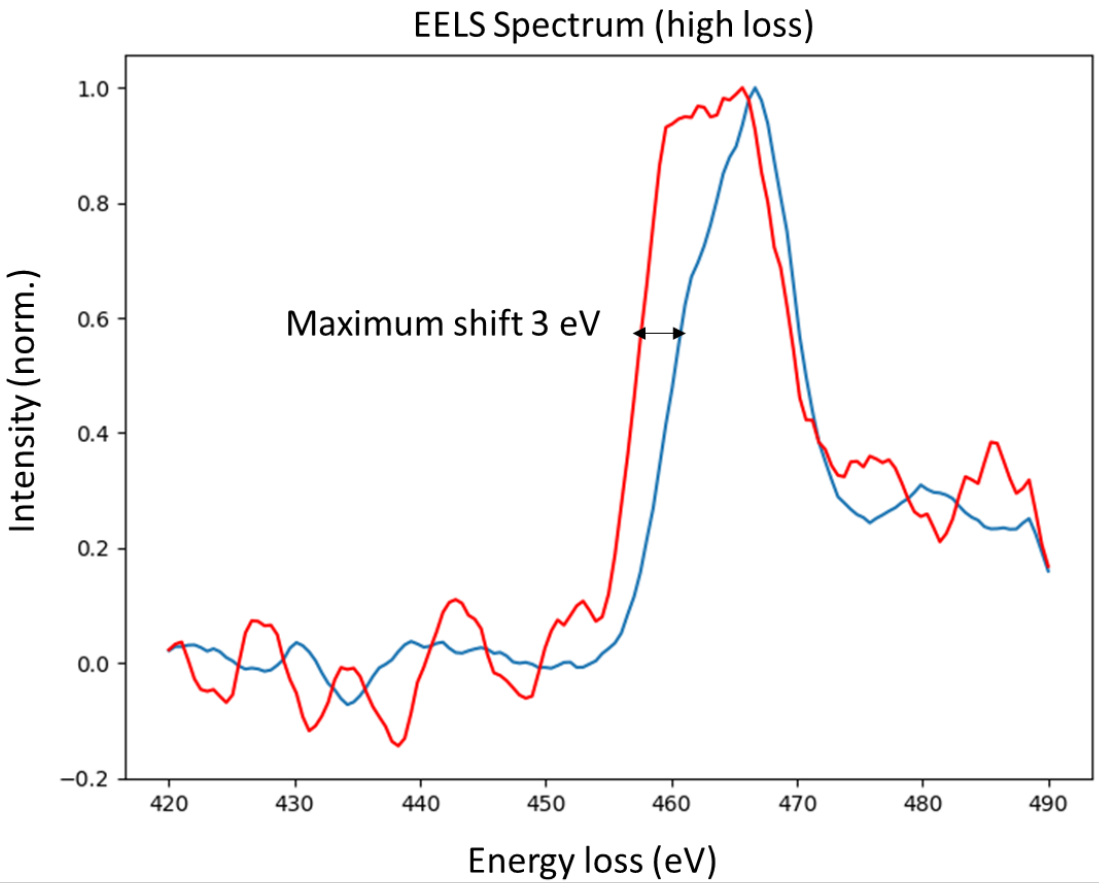

Figure S5: EELS spectrum showing the maximum energy shift that occurs in the atomic-scale spectrum image shown in Figure 12 d.

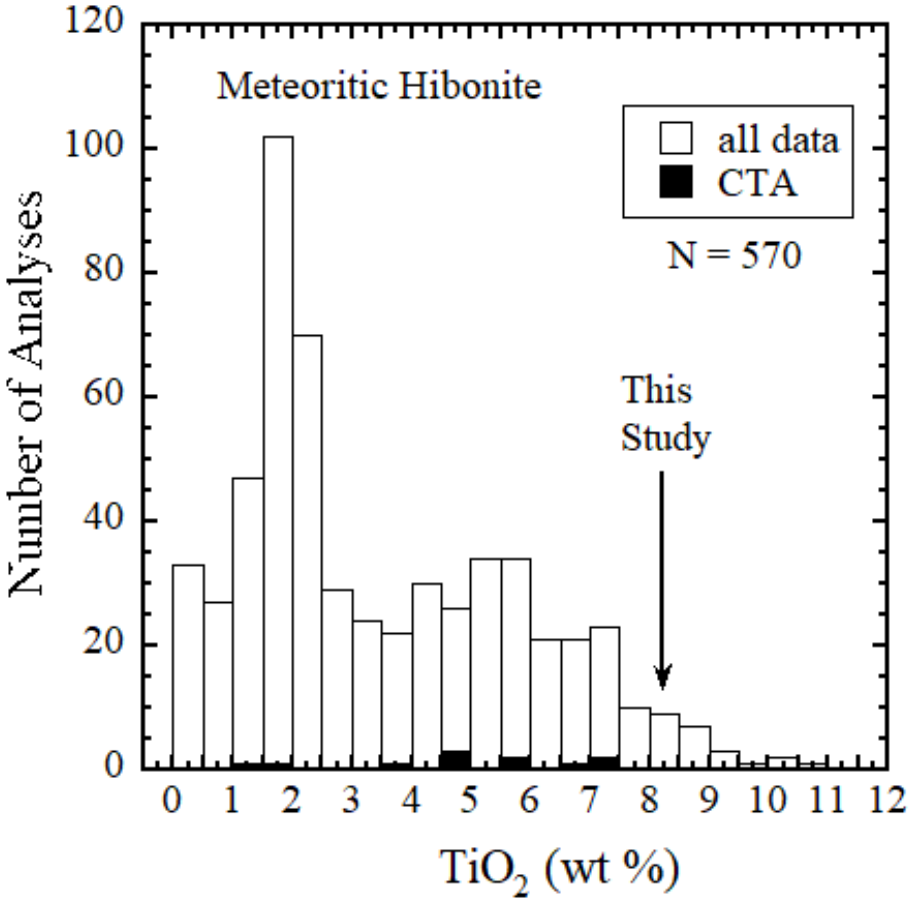

Figure S6: Concentration in TiO2 (wt. %) of previously measured meteoritic hibonites. The hibonite grain from this study, extracted from a CTA CAI, is shown by an arrow.

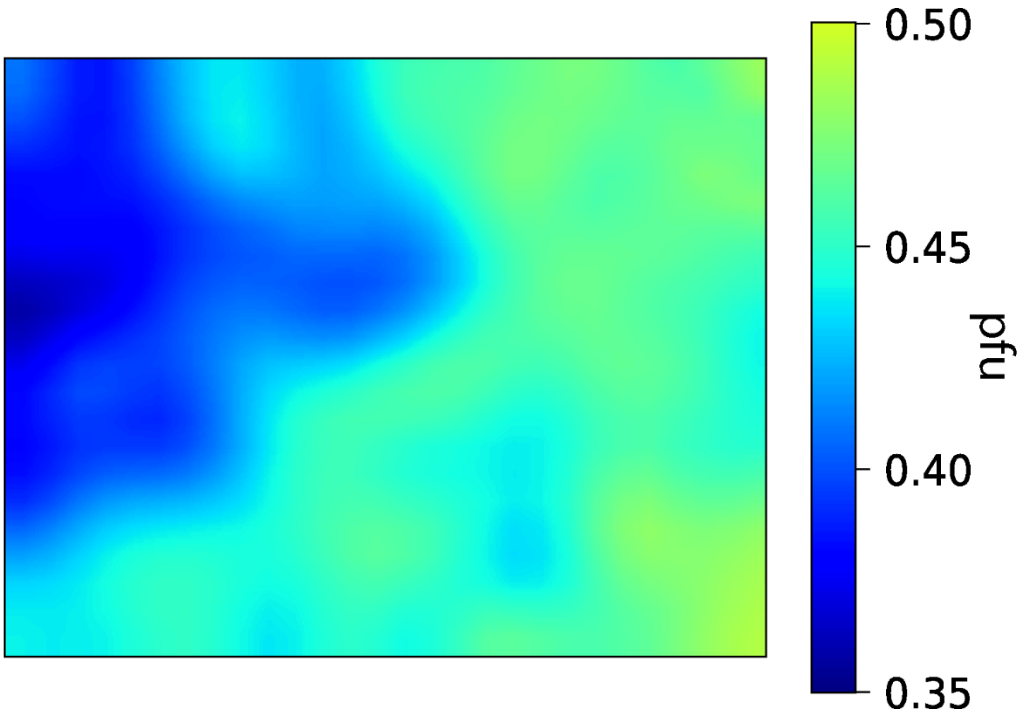

Figure S7: Oxygen vacancies calculated on the basis of the charge remaining after subtracting an ideal O_{19} charge from the charge of the cation sum. We assumed V=3+, Cr=3+, Fe=2+. There are more vacancies toward the edge of the grain (right side of image) and where the Ti^{3+} is the highest (Fig. 10).

We attribute the lack of electroneutrality to the presence of unmeasured oxygen vacancies. The fact that the Mg and Ti distributions do not correlate to the $Ti^{4+}/\Sigma Ti$ ratio distribution indicates that neither the direct substitution ($Ti^{3+} \rightleftharpoons Al^{3+}$), the coupled substitution ($Ti^{4+} + Mg^{2+} \rightleftharpoons 2Al^{3+}$), nor the sum of these reactions can explain the $Ti^{4+}/\Sigma Ti$ ratio distribution. Another reaction must have therefore produced the observed distribution, most likely in the solar protoplanetary disk. We suggest that this is an indirect measure of the oxygen vacancy in the sample. To obtain the oxygen vacancy concentration, the scale bar can be divided by two. A 0.5 oxygen vacancy in cation per formula unit represents 1/12 of the atoms on the O4 Wyckoff site which is the closest site to the M3 site where Mg substitutes.